Journal of Materials Chemistry A

Accepted Manuscript

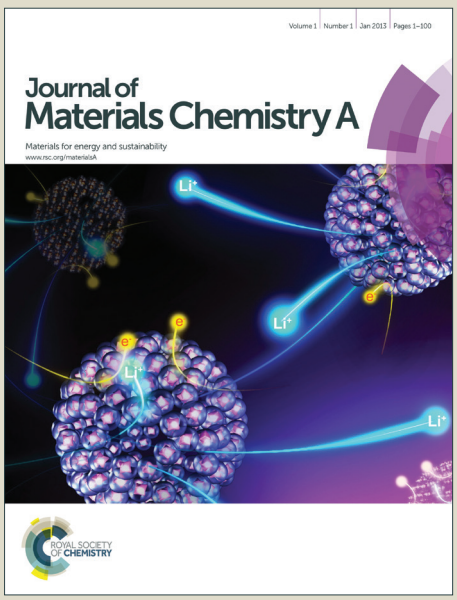

ROYAL SOCIETY OF CHEMISTRY

www.rsc.org/materialsA

Cite this: DOI: 10.1039/c0xx00000x

www.rsc.org/xxxxxx

ARTICLE TYPE

High sulfur loading composite wrapped by 3D nitrogen-doped graphene as cathode material for lithium-sulfur batteries

Chao Wang,[a,b] Kai Su,[b] Wang Wan,[b] Hua Guo,[b] Henghui Zhou,[b] Jitao Chen,*[b] Xinxiang Zhang[b] and Yunhui Huang*[a]

Received (in XXX, XXX) Xth XXXXXXXXX 20XX, Accepted Xth XXXXXXXXX 20XX
DOI: 10.1039/b000000x

A porous three-dimensional nitrogen-doped graphene (3D-NG) was introduced as an interconnected framework for sulfur in lithium-sulfur battery. The 3D-NG-sulfur composite (3D-NGS) with a high sulfur content of 87.6 wt% was synthesized via a facile one-pot solution method while sulfur was well dispersed within it. The as-designed 3D-NGS composite exhibits excellent rate capability and cyclability. The discharge specific capacity is 792 mAh g^{-1} after 145 cycles at a current density of 600 mA g^{-1} and the capacity fading rate is 0.05% per cycle. Even at a high rate of 1500 mA g^{-1}, the composite still shows a good cycle performance with a capacity of 671 mAh g^{-1} after 200 cycles. The outstanding electrochemical performance can be attributed to the flexible porous 3D structure and N-doping in graphene. The flexible 3D-NG can provide a conductive framework for electron transport and alleviate the volume effect during cycling; N-doping can facilitate the penetration of Li ions across the graphene and restrain sulfur due to the strong chemical bonding between S and nearby N atoms.

Introduction

Lithium-sulfur battery is an attractive and promising electrochemical device for future energy conversion and storage due to its abundant resource of sulfur, environment friendliness and superhigh theoretical capacity (1675 mAh g^{-1}).[1] Generally, the Li-S battery uses Li metal as anode. Considering the safety issue of Li anode, some researchers tried to use Li_2S to substitute Li metal as the anode, but the capacity of Li_2S is much lower.[2-4] Recently, many hopeful progresses have been achieved in Li-S batteries.[5-8] However, the rapid capacity decay is still the main limitation for application due to the low electrical conductivity of elemental sulfur (~5×10^{-30} S cm^{-1} at room temperature), large volume change[9] and high solubility of the intermediates (Li_2S_x, $x > 2$) in the organic electrolyte of the charge and discharge processes.[10] The solubility not only leads to the loss of active materials from the cathode, but also causes serious "redox shuttle" reactions between polysulfide (PS) anions in the electrolyte and Li metal anode, which resulting in poor electrochemical performance.[11] Conductive incorporation with carbon nanotubes, graphene or conductive polymers has been extensively introduced to suppress the solubility problem and hence to improve the electrochemical performance.[8, 12, 13] For example, graphene or graphene oxide (GO) can be used as conductive framework to fabricate sulfur composites with designed structure for superior performance.[4, 14] Many reports used to focus on the cells with very high specific capacity but low sulfur content.[15] In general, the lower the sulfur content, the higher the sulfur-based specific capacity is.[16, 17] Moreover, if a proper supporter is used for sulfur loading, the cyclability will be improved. Recent study showed that using hydroxylated graphene as supporter for sulfur with a content of 50 wt% gave a capacity retention of 84% after 100 cycles.[18] However, low sulfur content greatly reduces the overall volumetric capacity and energy density of the cathode.[16, 17] A superior Li-S battery should requests a high sulfur loading and at the same time show excellent electrochemical performance.[19]

Graphene, one-atom-thick layers of sp^2-hybridized carbon atoms packed in a honeycomb lattice, is renowned for its fascinating electronic properties and potential applications in energy conversion and storage in lithium-ion batteries (LIBs).[20] So far, both theoretical and experimental studies have demonstrated that the intentional incorporation of heteroatoms into graphene structure can effectively modify its electronic and chemical properties.[21] Continuous efforts have been done to fabricate doped graphene. The nitrogen-doped, boron-doped and sulfur-doped graphene are commonly used in fuel cells and LIBs, which exhibit good electrochemical performance.[22] The reason for the performance improvement lies in that the doped atoms with different electronegativity can break the electroneutrality of graphene to create the charged

sites and increased conductivity which can enhance the discharge and charge capacity of graphene in LIBs. It is also recognized that integration of 2D graphene sheet into 3D macroscopic structure may pave a way towards high performance for practical application. Usually hydrothermal and solvothermal treatment of GO is an efficient method to form 3D-GO.[23]

In this work, we introduced a 3D-NG framework as the supporter of sulfur to form the 3D-NG sulfur (3D-NGS) composite. The scheme of fabrication is illustrated in Fig. 1. The graphene oxide was assembled into a porous 3D structure during the solvothermal process. The N-doped graphene serves as a good

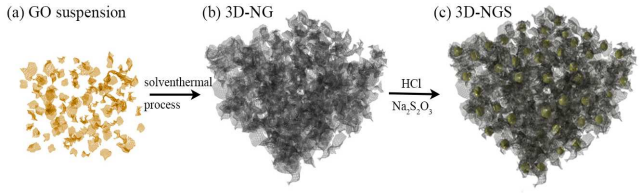

Fig. 1 Schematic illustration for synthesis process of the 3D-NGS composite: (a) GO suspension, (b) 3D-NG obtained from GO through a solvothermal process, and (c) the final 3D-NGS composite.

electron conductive framework and sulfur stabilizer. The foam-like NG can load a high content of sulfur (87.6 wt%); the sulfur particles are well distributed into the 3D framework. Such 3D structure is a very good conductive network to envelope sulfur and to improve the insulation nature of sulfur, while the NG provides highly reactive functional groups at its surface to hold sulfur and trap polysulfides during discharge-charge process. The electrochemical performance of the N-doped and undoped sulphur-based composites were investigated. Our investigation shows that the uniform loading of S in the 3D-NG is an efficient route to attain superior performance.

Experiment section

Materials synthesis

Synthesis of GO

GO was prepared from expanded graphite powder by a modified Hummers method.[22] Typically, 2 g graphite, 1 g $NaNO_3$ and 50 ml concentrated sulfuric acid were mixed together and stirred at room temperature for 24 h. The mixture solution was put into ice bath under vigorous stirring, followed by drop addition of 6 g $KMnO_4$. Subsequently, the solution was transferred to a water bath at 35–40 °C and kept for 30 min. After that, 90 ml distilled water was gradually added for three times; each time the solution was stirred for 15 min. The obtained solution was diluted with 280 ml water and treated with 20 ml H_2O_2 (30%). The color turned from dark brown to bright yellow. The warm solution was filtered, and washed successively with 5% HCl solution and water. A resultant GO gel was attained by centrifugation at 20,000 rpm.

Synthesis of 3D-NG

3D-NG was synthesized through a one-pot solvothermal process. In a typical procedure, 2 g GO gel with a concentration of 20 mg ml^{-1} was added into 10 ml water and sonicated for 0.5 h. Then, 30 ml ammonia solution (25 wt% in water) was added. The mixture was transferred into a 50 ml Teflon-lined autoclave and maintained at 200 °C for 12 h. The 3D-NG hydrogel was formed, and washed with water and ethanol repeatedly. The final product was collected by frozen drying.

Synthesis of 3D-NGS and GO-S

The 3D-NGS composite was synthesized via a facile one-pot solution route by just using sodium thiosulfate and hydrochloric acid. In a typical procedure, 0.1 g NG was dispersed into the solution, and sonicated for 10 min. Thereafter, 6.9 g $Na_2S_2O_3$ was added and stirred for 10 min. After that, 2.7 g concentrated HCl that was diluted into 0.05 mol l^{-1} aqueous solution was added dropwise at a rate of 10 ml min^{-1} to the above solution and stirred for 10 min. The composite was collected by vacuum filtration. The precipitated 3D-NGS material was washed by water repeatedly. The final composite product was obtained by drying at 60 °C overnight. For comparison, a reference GO-S composite was synthesized via the same precipitation route.

Materials characterization

The phase of the 3D-NGS composite was checked by X-ray diffraction (XRD) on a Rigaku D/MAX-2000 diffractometer (Japan) using Cu Kα radiation (λ = 0.15406 nm) from 2θ = 10° to 70°. The morphology and microstructure were observed by field-emission scanning electron microscope (SEM, S4800, Hitachi). The elemental mapping was conducted via local chemical analysis performed by energy dispersive X-ray spectroscopy (Team EDS). The component ratio of the composite was determined by thermogravimetric analysis (Mettler Toledo) in the temperature range of 25–400 °C at a heating rate of 5 °C min^{-1} under N_2 atmosphere. The chemical transformation of the composite during the preparation process was investigated by Fourier transform infrared spectroscopy (FTIR, Bruker VECTOR22) with KBr pellets. The N content in the composite was determined by chemical elemental analysis (CHNS, Vario EL, Elementar). X-ray photoelectron spectroscopy (XPS) measurements were carried out on an Axis Ultra (Kratos Analytical Ltd.) imaging photoelectron spectrometer using a monochromatized Al Ka anode. Brunauer–Emmett–Teller (BET) surface area was measured at 77 K through N_2 adsorption/desorption isotherms by a

Micromeritics ASAP 2010 analyzer.

Electrochemical measurements

The electrochemical properties of the composites were evaluated by using coin cells with lithium metal as anode and Celgard 2400 film as separator. The cathode was prepared by mixing the active material, acetylene black and polyvinylidene fluoride (PVDF) binder in a weight ratio of 70:20:10 in N-methylpyrrolidone to form homogeneous slurry. The slurry was uniformly spread onto pure aluminium foil with a doctor blade cast, and dried at 60 °C for 12 h in a vacuum. The electrode was punched into circular disks with diameter of 12 mm with active-material loading of about 1 mg cm^{-2}. CR2032 coin cells were assembled in an argon-filled glove box (Master 100 Lab, Braun, Germany). 0.6 mol l^{-1} LiTFSI/DOL + DME (1 : 1 by volume) was used as electrolyte and 0.4 mol l^{-1} $LiNO_3$ as additive. Cells were galvanostatically charged and discharged between 1.7 and 2.8 V versus Li^+/Li on a Land CT2001A battery tester. The specific capacities and current rates were calculated based on the mass of S in the cathode. Electrochemical impedance spectroscopy (EIS) was performed on the coin cell by electrochemical workstation (Autolab PG302N, Netherlands) with an applied sinusoidal excitation voltage of 5 mV in the frequency range from 100 kHz to 0.01 Hz. Electronic conductivity was tested by linear sweep method through Autolab PG302N.

Results and discussion

The self-assembled 3D-NG was synthesized through a facile solvothermal process of GO by only using ammonia solution. Compared with some common reductants like hydrazine and sodium borohydride, the ammonia solution serves as both reducing agent and nitrogen source rather than a regulator to adjust the pH value of the solution. Therefore, the method we developed here is more convenient, safe and economical.

The self-assembled 3D-NG was solvothermally formed from 2 mg ml^{-1} GO suspension at 200 °C in a Teflon-lined autoclave. Photograph of the as-synthesised 3D-NG is shown in Fig. 2a, and its corresponding SEM image is shown in Fig. 2b. It can be seen that the graphene was incorporated in an interconnected, porous 3D framework with continuous micron macropores. Measured by a Micromeritics ASAP 2010 analyzer, the specific BET surface area of the 3D-NG sample was 398 m^2 g^{-1}. It is observed from Fig. S1 that the pore size was mainly distributed at around 4 nm. The large BET surface area and the 3D structure can provide enough space for loading and volume expansion of sulfur.

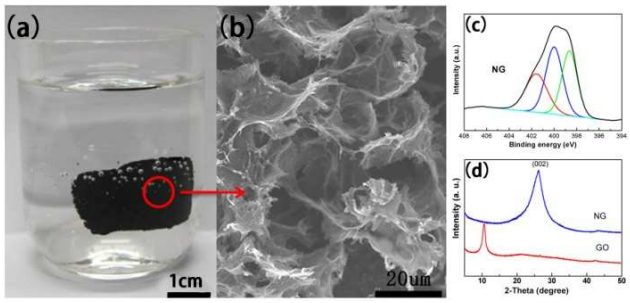

Fig. 2 (a) Photograph of the 3D-NG hydrogen soaked in water and ethanol mix liquid after hydrothermal process at 200 °C for 12 h. (b) SEM images of 3D-NG framework. (c) The N 1s XPS spectrum of 3D-NG. (d) XRD patterns of GO (red) and 3D-NG (blue).

Several reports have demonstrated that NG has a better electron transfer efficiency than pristine GO.[24-26] Our results also confirm this conclusion. The 3D-NG in our case showed an electronic conductivity of 1.02 S cm^{-1}, indicating that it is a promising conductive supporter for the sulfur electrode.

XRD analysis was employed to check the structures of GO and 3D-NG. As shown in Fig. 2d, a peak centred at 2θ = 10.6° of GO corresponds to a layer distance of 0.83 nm, which is related with the introduction of various oxygen-containing groups. After solvothermal treatment, the peak shifted to 2θ = 26.6° that can be assigned to the (002) plane of graphite, further proving the reduction of GO.

FTIR was used to analyse the chemical compositions of GO and NG (Fig. S2). GO showed a typical spectrum, as described in detail in ESI†. After solvothermal treatment, the content of the oxygen-containing groups in GO significantly decreased, while two new N-related peaks appeared at 1458 and 1543 cm^{-1} of NG, which can be preliminarily assigned to C–N stretching and N–H bending bonds of amide, respectively.[22] To future investigate the N-doping effect in graphene, XPS measurement was carried out. The N 1s XPS spectrum of NG is displayed in Fig. 1c. Generally, the peaks located at 398.6, 400.0, 401.5 eV are assigned to pyridinic-, pyrrolic-, and graphitic-type of N atoms doped in the graphene structure.[23] It can be seen that the pristine GO was adequately reduced and efficiently doped by N atoms. N content in the 3D-NG was determined to be 10.1 at.% (33.9% pyridinic, 37.9% pyrrolic, and 28.2% graphitic N). As we know, the performance of N-graphene can be influenced by many factors, such as types of the introducd N atoms, defects, disordered surface morphology induced by doping, and electrode/electrolyte wettability, etc.[13] Notably, it revealed that both the pyridinic and graphitic N play important roles in lithium-ion intercalation and extraction. Graphitic N-doping shows a lower diffusion barrier for the diffusion of Li atoms in graphene.[27]

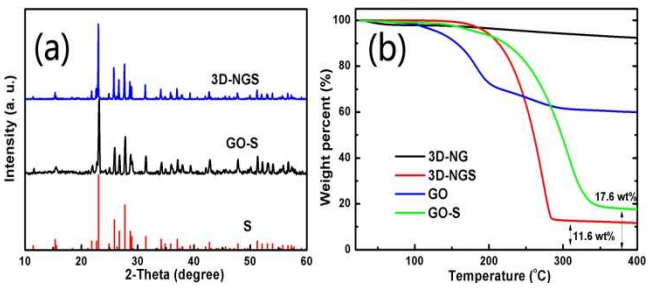

Fig. 3 (a) XRD patterns of S, GO-S and 3D-NGS; (b) TG curves for 3D-NG, 3D-NGS, GO, and GO-S from room temperature to 400 °C at a heating rate of 5 °C min^{-1} under N_2 atmosphere.

The GO-S and 3D-NGS composites were both synthesized by a facile one-pot solution route just using sodium thiosulfate and hydrochloric acid. The normalized XRD patterns of the 3D-NGS and GO-S shown in Fig. 3a agree well with the patterns of standard sulfur (JCPSD No. 08-0247). It is noteworthy that no graphite or graphene oxide peaks appeared in the patterns, which demonstrates that the graphene sheets are in a substantially exfoliated state and do not re-stack upon in the synthesis process.

The sulfur contents in 3D-NGS and GO-S were determined TG measurement and chemical elemental analysis. It can be seen in Fig. 3b that the weight losses of 3D-NGS, GO-S at 400 °C were 88.4 wt% and 82.4 wt%. NG and GO show a weight loss of 9 wt% and 40 wt% during the process, indicating that the content of oxhydryl and carboxyl in GO was much larger than 3D-NG. According to the weight loss and N content in 3D-NGS (1.05 wt%), we calculated that the S content of 3D-NGS was 86.7 wt%. The sulfur content in our case is almost the highest as compared with many other reports.[28] Low sulfur content in cathode material is the main problem to restrain the development of Li-S battery. High S loading is a promising way to improve the performance of sulfur cathode materials.[29, 30] Based on the weight loss of GO, we also obtained that the sulfur content in GO-S was 75 wt%. The very high S content in 3D-NGS can be contributed not only to the good loading effect of the porous 3D structure, but also to the additional active sites to hold the sulfur from the doped N atoms, which was confirmed by theoretical calculation.[31] It should be mentioned that synthesis conditions of the composites are also important to the sulfur holding, which need optimization in the experiment.

The morphologies of the GO-S and 3D-GNS composites were investigated by SEM. Figs. 4a, b show the SEM images of GO-S composite. We can see that some sulfur particles were enveloped by graphene sheet but most of the sulfur particles were uncovered. The size of sulfur particles was about 2 μm. The morphology of the 3D-GNS composite is shown in Fig. 4c, d. Almost no exposed sulfur was observed and the original graphene sheet was curled to wrap sulfur inside and the size of sulfur particle was similar to the GO-S composite's, i.e., about 2 μm. More images of 3D-NGS can be seen in Fig. S4. We wonder why the N-doped graphene has a much better coating effect than graphene oxide.

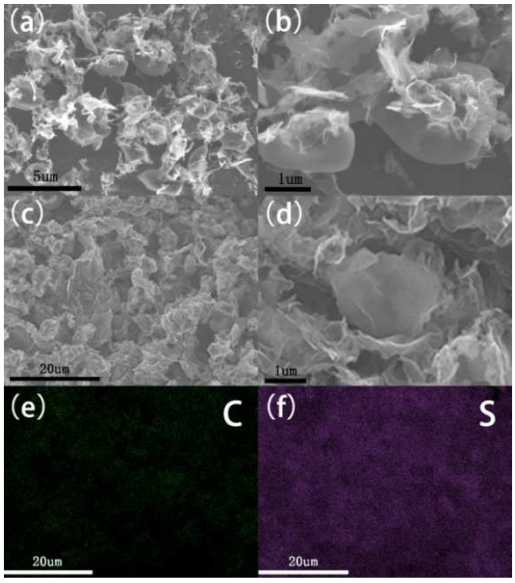

Fig. 4 SEM image of the microstructure of GO-S composite (a), (b) and 3D-NGS composite (c), (d). Corresponding elemental mapping of 3D-NGS (c) for the distribution of C (e) and S (f).

Surface modification can improve the binding energy of sulfur and the carbon substrate.[5] From FTIR and TG results, we can conclude that the –OH and –COOH contents of GO are much larger than NG. Since sulfur and graphene both are nonpolar molecules, the existence of –OH and –COOH at the graphene surface can reduce the molecular interaction between sulfur and graphene, hence prevent the contact between sulfur and graphene during the synthesis process. If nitrogen is doped during the hydrothermal process, the amount of –OH and –COOH groups may decrease greatly while the nitrogen is incorporated. The scheme of the N-doped graphene is shown in Fig. S3. The decrease of –OH and –COOH leads to the enhanced intermolecular force of sulfur and graphene, since they are nonpolar molecules according to the similarity principle. Moreover, the intermolecular force between sulfur and graphene is dispersion force. When nitrogen is doped, each N atom provides two electrons in graphene conjugated system, so the dispersion force is larger than the undoped one. Therefore, the interaction between sulfur and NG is much stronger than that between sulfur and GO. Wang et al. used the first principle to study the N-doped effect, showing that a strong binding can be formed between the sulfur atoms and the nearby N atoms in the N-doped system.[31]

XPS analysis of 3D-NGS is shown in Fig. S5. The peaks centered at 163.9 and 164.9 eV are the evidences of C-S and S-O bonding which may cause the intending deposition of sulfur on the graphene surface.[32] With growth of sulfur particles, NG was curled and covered on the surface of sulfur. The strong binding between sulfur and carbon facilitates the enfolding of graphene sheet on sulfur. Meanwhile, the presence of such chemical bonding can immobilize sulfur and prevent the diffusion of polysulfides during discharge charge and charge processes.[33, 34] The corresponding elemental analysis for C and S in the 3D-NGS composite (Fig. 4c) is shown in Fig. 2e, f. Clearly, the C and S species are homogeneously distributed in the composite.

The electrochemical properties of 3D-NGS and GO-S composites were examined by a 2032 coin cell. All the cells ran at a current density of 100 mA g^{-1} for the first two cycles. Fig. S6 shows the cycling performance and coulombic efficiency of 3D-GNS at a current density of 250 mA g^{-1}. After 80 cycles, the capacity still maintained at 936 mAh g^{-1}. However, the cycling performance of GO-S composite was much worse as compared with 3D-NGS under the same condition. After 200 cycles, the capacity decreased from 859 mAh g^{-1} to 370 mAh g^{-1} (Fig. S7).

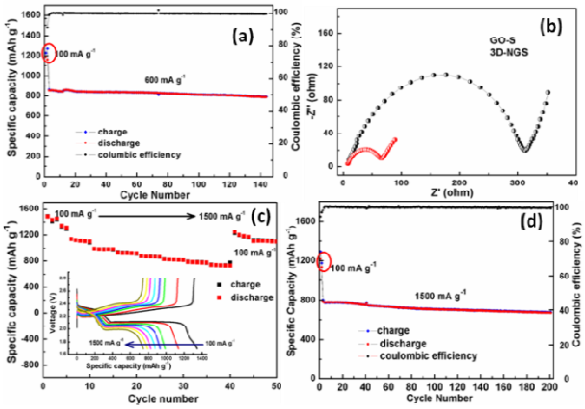

Fig. 5 Electrochemical performance of 3D-NGS composite. Cycling stability and corresponding coulombic efficiency of 3D-NGS at a current density of 100 mA g^{-1} at the first two cycles and 600 mA g^{-1} (a) and 1500 mA g^{-1} (d) at the following cycles. (b) EIS of the GO-S and 3D-NGS composites with an applied sinusoidal excitation voltage of 5 mV in the frequency range from 100 kHz to 0.1 Hz. (c) Rate capability of 3D-NGS with a current density ranging from 100 mA g^{-1} to 1500 mA g^{-1} and the first discharge-charge profile at different current densities.

We further examined the cycling performance of 3D-GNS at 600 mA g^{-1} (see Fig. 5a). After 145 cycles, it showed a reversible capacity of 792 mAh g^{-1}, indicating a capacity fading rate of 0.05% per cycle, much lower than many reports for the sulfur cathode at high rate.[34-36] The corresponding charge and discharge profiles at 5th, 50th, and 100th cycles are shown in Fig. S8. It is typical for the Li-S cells to show two discharge and one charge voltage plateaus. The two discharge voltage plateaus observed at ~2.35 and ~2.1 V are assigned to the two-step reaction during discharge process, corresponding to the reduction from S_8 to long chain lithium polysulfides (Li_2S_x, $4 < x < 8$) and further from polysulfides to Li_2S_2 or Li_2S. With the proceed of cycling at the first few cycles, the charge plateau decreased, and the discharge plateaus increased, indicated that the polarization between the charge and discharge plateaus diminished, and the plateaus keep the same even after 100 cycles exhibiting good stability.

The high capacity retention of the 3D-NGS composite can be ascribed to the good reversibility of the 3D framework. The flexible framework can provide enough space for the volume change during charge and discharge processes.[37] The electrode exhibited a coulombic efficiency near 100% during cycling, demonstrating that the sulfur shuttle phenomenon was controlled effectively to a quite low level. It is believed that the 3D-NG acts as a sulfur immobilizer and the function groups on the graphene surface can restrain polysulfides.[25] Combined with the use of $LiNO_3$, the cell shows a very high coulombic efficiency.

We examined the conductivity of the sulfur composites using electrochemical impedance spectroscopy (EIS) (Fig. 3b). The diameter of the semicircular portion of the curve represents the charge transfer resistance R_{ct}. The R_{ct} values of the NG and GO composites were 88 and 352 Ω cm^{-2}, respectively (electrode area was normalized). It is obvious that the NG composite electrode exhibited a much lower charge transfer resistance than that of the GO composite, which could be attributed to the enhanced conductivity of the NG composite.

To further investigate the electrochemical performance, we tested the rate capability of 3D-NGS at various current densities from 100 to 1500 mA g^{-1} (Fig. 5c). The composite exhibited excellent rate performance with reversible specific capacities of 1483, 1134, 990, 931, 875, 828, 785 and 743 mAh g^{-1} at 100, 200, 400, 600, 800, 1000, 1200, and 1500 mA g^{-1}, respectively. The charge and discharge capacities were almost the same indicating good coulombic efficiency. Moreover, the superior performance of 3D-NGS can also be evidenced by the easy recovery of the capacity after cycling. The capacity was recovered up to 1227 mAh g^{-1} and stabilized at 1120 mAh g^{-1} when the current density was tuned back to 100 mA g^{-1} after cycling at various currents. For comparison, the rate performance of GO-S is given in Fig. S9. It can be seen that, the specific capacity keeps at 700 mAh g^{-1} when the current densities were below 400 mA g^{-1}, but it faded to 270 mAh g^{-1} as soon as the current density increased to 800 mA g^{-1}, indicative of a much worse rate performance as compared with 3D-NGS. The capacity retention at various current densities was not as high as the N-

doped sample. The inserted graph in Fig. 5c shows the charge and discharge voltage profiles at corresponding current density. We can see that the change of charge and discharge plateaus were very small even at high current rates. 3D-NGS shows really good electrochemical performance. This may be due to the decrease of energy barrier for Li ions to penetrate the N-doped graphene as compared with the undoped one. Therefore, the N-doping in graphene is favourable for the penetration of Li ions.[31]

The cycle performance was also examined at a high current density of 1500 mA g^{-1}. After being charged and discharged at 100 mA g^{-1} at the first two cycles, the cell showed a very good capacity retention (85.6%) which maintained a reversible capacity of 672 mAh g^{-1} after 200 cycles at 1500 mA g^{-1}. The coin cells were disassembled to check the change of separators. The cells of GO-S were operated under the same condition. From Fig. S10, we can see that the color of separator was changed especially for the GO-S one. Color change is mainly due to the dissolution of polysufides into the electrolyte. The high the solubility, the deeper the color is. The separator of 3D-NGS was slightly yellow and small black spots were observed, whereas for the GO-S one the color was much darker and many black spots appeared on the separator. Such difference is consistent with the report that S atoms can be encapsulated inside the N-doped graphene because of the strong chemical bonding between S and N atoms.[3] This further improves the efficiency of polysulfides trap in the porous 3D N-doped structure of graphene. After the cells were disassembled, we observed some cracks on the surface of the GO-S electrode, but no crack appeared on the surface of the 3D-NGS. The cracks were mainly caused by the volume change during cycling. The phenomenon demonstrates that the 3D framework can alleviate the volume change of the composite during cycling.

The excellent electrochemical performance in the 3D-NGS can be explained by the good conductivity of the 3D framework and the high chemical interaction between S and 3D-NG containing functional groups. These characteristics allow fast transport for lithium ions and electrons through the network. Moreover, the porous 3D structure can effectively entrap polysulfides during cycling. Therefore, the 3D-NGS composite shows excellent rate capability and long cyclic performance at various currents.

Conclusions

A novel sulfur cathode composite of 3D-GNS with sulfur loading as high as 87.6 wt% was synthesized through a facile solution route. Even with this very high sulfur content, the composite still showed outstanding electrochemical performance. A reversible discharge capacity of 792 mAh g^{-1} was retained and capacity retention of 92.5% was obtained after 145 cycles at a current density of 600 mA g^{-1}. Moreover, the 3D-GNS exhibited excellent rate capability and high coulombic efficiency. The superior electrochemical performance can be attributed to the flexible porous 3D structure and N-doping. The porous 3D structure can not only provide enough space for volume change of sulfur to diminish the volume expansion effect, but also trap polysulfides effectively; N-doping in graphene can facilitate fast transport for both electrons and Li ions. We believe that such 3D-NG composite is also applicable for the electrode materials in lithium-ion batteries or other energy storage devices.

Acknowledgements

The authors gratefully acknowledge the financial support by the Natural Science Foundation of China (Grant No. 51361130151) and the National High-Tech Research and Development Program of China (863 program) (Grant No. 2013AA119102).

Notes and references

[a] *Key Laboratory for Advanced Battery Materials and System (MOE), School of Materials Science and Engineering, Huazhong University of Science and Technology (HUST), Wuhan, Hubei 430074, China Fax:86-27-87558241;Tel:86-27-87558241;E-mail: huangyh@mail.hust.edu.cn*

[b] *College of Chemistry and Molecular Engineering, Peking University, Beijing, P. R. China. Fax: 86-10-62754680; Tel: 86-10-62754680; E-mail: chenjitao@pku.edu.cn*

†Electronic Supplementary Information (ESI) available: experiment data including pore size distribution, FTIR, XPS and some electrochemical data. See DOI: 10.1039/b000000x/.

‡ Footnotes should appear here. These might include comments relevant to but not central to the matter under discussion, limited experimental and spectral data, and crystallographic data.

1. X. Ji, K. T. Lee and L. F. Nazar, Nat. Mater., 2009, 8, 500-506.
2. K. Cai, M. K. Song, E. J. Cairns and Y. Zhang, Nano Lett., 2012, 12, 6474-6479.
3. Y. Yang, G. Zheng, S. Misra, J. Nelson, M. F. Toney and Y. Cui, J. Am. Chem. Soc., 2012, 134, 15387-15394.
4. S. Evers and L. F. Nazar, Acc. Chem. Res., 2013, 46, 1135-1143.
5. G. Zheng, Q. Zhang, J. J. Cha, Y. Yang, W. Li, Z. W. Seh and Y. Cui, Nano Lett., 2013, 13, 1265-1270.
6. J. T. Lee, Y. Zhao, S. Thieme, H. Kim, M. Oschatz, L. Borchardt, A. Magasinski, W. Cho, S. Kaskel and G. Yushin, Adv. Mater., 2013, 25, 4573-4579.
7. C. Wang, W. Wan, J. Chen, H. Zhou, X. Zhang, L. Yuan and Y. Huang, J. Mater. Chem. A, 2013, 1, 1716-1721.
8. R. Chen, T. Zhao, J. Lu, F. Wu, L. Li, J. Chen, G. Tan, Y. Ye and K. Amine, Nano Lett., 2013, 13, 4642-4649.
9. Y. Yang, G. H. Yu, J. J. Cha, H. Wu, M. Vosgueritchian, Y. Yao, Z. A. Bao and Y. Cui, ACS Nano, 2011, 5, 9187-9193.
10. Y. Yang, G. Zheng and Y. Cui, Energy Environ. Sci., 2013, 6, 1552-1558.

11. J. Akridge, Solid State Ionics, 2004, 175, 243-245.
12. L. Xiao, Y. Cao, J. Xiao, B. Schwenzer, M. H. Engelhard, L. V. Saraf, Z. Nie, G. J. Exarhos and J. Liu, Adv. Mater., 2012, 24, 1176-1181.
13. A. Manthiram, Y. Fu and Y. Su, Acc. Chem. Res., 2012, 46, 1125-1134.
14. G. Li, G. Li, S. Ye and X. Gao, Adv. Energy Mater., 2012, 2, 1238-1245.
15. W. Weng, V. G. Pol and K. Amine, Adv. Mater., 2013, 25, 1608-1615.
16. S. Evers and L. F. Nazar, Chem. Commun., 2012, 48, 1233-1235.
17. L. Yin, J. Wang, F. Lin, J. Yang and Y. Nuli, Energy Environ. Sci., 2012, 5, 6966-6972.
18. C. Zu and A. Manthiram, Adv. Energy Mater., 2013, 3, 1008-1012.
19. Y. Yang, G. Zheng and Y. Cui, Chem. Soc. Rev., 2013, 42, 3018-3032.
20. Q. Tang and Z. Zhou, Prog. Mater Sci., 2013, 58, 1244-1315.
21. Q. Tang, Z. Zhou and Z. Chen, Nanoscale, 2013, 5, 4541-4583.
22. C. Zhang, R. Hao, H. Liao and Y. Hou, Nano Energy, 2013, 2, 88-97.
23. C. Barchasz, F. Molton, C. Duboc, J. Leprêtre, S. Patoux and F. Alloin, Anal. Chem., 2012, 84, 3973-3980.
24. D. Usachov, O. Vilkov, A. Grüneis, D. Haberer, A. Fedorov, V. K. Adamchuk, A. B. Preobrajenski, P. Dudin, A. Barinov, M. Oehzelt, C. Laubschat and D. V. Vyalikh, Nano Lett., 2011, 11, 5401-5407.
25. Y. Wang, Y. Shao, D. W. Matson, J. Li and Y. Lin, ACS Nano, 2010, 4, 1790-1798.
26. H. Wang, T. Maiyalagan and X. Wang, ACS Catalysis, 2012, 2, 781-794.
27. D. H. Wu, Y. F. Li and Z. Zhou, Theor. Chem. Acc., 2011, 130, 209-213.
28. D. Wang, Q. Zeng, G. Zhou, L. Yin, F. Li, H. Cheng, I. R. Gentle and G. Q. M. Lu, J. Mater. Chem. A, 2013, 1, 9382-9394.
29. S. S. Zhang and J. A. Read, J. Power Sources, 2012, 200, 77-82.
30. S. S. Zhang and D. T. Tran, J. Power Sources, 2012, 211, 169-172.
31. Z. Wang, X. Niu, J. Xiao, C. Wang, J. Liu and F. Gao, RSC Adv., 2013, 3, 16775-16780.
32. L. Wang, D. Wang, F. Zhang and J. Jin, Nano Lett., 2013, 13, 4206-4211.
33. L. Ji, M. Rao, H. Zheng, L. Zhang, Y. Li, W. Duan, J. Guo, E. J. Cairns and Y. Zhang, J. Am. Chem. Soc., 2011, 133, 18522-18525.
34. H. Wang, Y. Yang, Y. Liang, J. T. Robinson, Y. Li, A. Jackson, Y. Cui and H. Dai, Nano Lett., 2011, 11, 2644-2647.
35. Y. Cao, X. Li, I. A. Aksay, J. Lemmon, Z. Nie, Z. Yang and J. Liu, Phys. Chem. Chem. Phys., 2011, 13, 7660-7665.
36. N. Li, M. Zheng, H. Lu, Z. Hu, C. Shen, X. Chang, G. Ji, J. Cao and Y. Shi, Chem. Commun., 2012, 48, 4106-4108.
37. G. Zhou, L. Yin, D. Wang, L. Li, S. Pei, I. R. Gentle, F. Li and H. Cheng, ACS Nano, 2013, 7, 5367-5375.